Appendix A.

Supplementary Material for

Influence of urban extent discrepancy on the estimation of surface urban heat island intensity: a global-scale assessment in 892 cities

Qiquan Yang [a, b, c], Yi Xu [a, *], Xiaohua Tong [b, c, *], Ting Hu [d, *], Yue Liu [e], TC Chakraborty [f], Rui Yao [g], Changjiang Xiao [b, c], Shurui Chen [b], Zonghan Ma [h]

[a] State Key Laboratory of Lunar and Planetary Sciences, Macau University of Science and Technology, Macau, China

[b] College of Surveying & Geo-Informatics, Tongji University, Shanghai, 200092, China

[c] The Shanghai Key Laboratory of Space Mapping and Remote Sensing for Planetary Exploration, Tongji University, Shanghai, 200092, China

[d] School of Remote Sensing and Geomatics Engineering, Nanjing University of Information Science and Technology, Nanjing, 210044, China

[e] Guangzhou Institute of Geography, Guangdong Academy of Sciences, Guangzhou, 510070, China

[f] Atmospheric Sciences and Global Change Division, Pacific Northwest National Laboratory, Richland, WA, USA

[g] School of Remote Sensing and Information Engineering, Wuhan University, Wuhan, 430079, China

[h] State Key Laboratory of Remote Sensing Science, Aerospace Information Research Institute, Chinese Academy of Sciences, Beijing, 100101, China

* Corresponding author. E-mail address: yixu@must.edu.mo (Yi Xu); xhtong@tongji.edu.cn (Xiaohua Tong); hutingrs@nuist.edu.cn (Ting Hu)

Text A.1. Descriptions of five global urban extent products used in this study

The urban extents of Global Human Settlement Layer (GHSL) are delineated as the spatially-generalized dense groupings of adjacent grid squares measuring 1 km^2, exhibiting a population density of no less than 1500 residents per km^2 of land surface or a minimum of 50% coverage of built-up surfaces per km^2 of land surface, along with a requisite populace of at least 50000 individuals (Florczyk et al. 2019). The GHSL product includes over 10,000 urban centers worldwide, providing important basic data for large-scale urban heat island studies (Tuholske et al. 2021; Venter et al. 2021).

The extraction of Global Urban Boundary (GUB) relies on the 30-m resolution global artificial impervious area produced by Gong et al. (2020). This data was firstly transformed into a kernel density map using the kernel density estimation technique. Regions exhibiting kernel density values surpassing 20% were classified as urban zones. Subsequently, the urban extents were derived through morphological operations (specifically dilation and erosion), followed by post-processing steps such as elimination of small clusters and inner holes (Li et al. 2020). The GUB shows advantages in terms of spatial resolution, and has been widely used in recent SUHI studies (Du et al. 2021; Hu et al. 2022; Liu et al. 2022b; Yang et al. 2021)

The MODIS land cover product (MCD12Q1, referred as MCD) is obtained by a decision tree classification of the supervised learning method and contains five different land cover classification schemes (Sulla-Menashe and Friedl 2018). In this study, the categorizations employed stem from the International Geosphere-Biosphere Programme (IGBP) framework. This categorization system encompasses a total of 17

distinct land cover categories. The classification labeled as the “Urban and Built-up Lands” is used to delineate urban extents (Sulla-Menashe and Friedl 2018). The MCD product can provide annual global urban extents from the year of 2001, and has long been an important data source for urban heat island studies (Chakraborty and Lee 2019; Clinton and Gong 2013; Liao et al. 2022; Liu et al. 2022a; Peng et al. 2012; Yao et al. 2019).

The global Morphological Urban Area (MUA), similar to above products, is produced mainly based on the artificial impervious surface data. However, the MUA product is unique because its urban area is extracted from the perspective of morphological characteristics. The core idea is to assume that urban boundaries can be determined by the morphological settlement index along the urban-rural transition (Taubenböck et al. 2019). The MUA product focuses primarily on the morphological characteristics of urban extents, and provides a new viewpoint for urban heat island studies (Taubenböck et al. 2019).

Unlike all the above GUEPs, the global datasets of Nighttime-Light-based Urban Area (NLUA) is extracted from nighttime light images. Compared with traditional remotely sensed satellite observations, the nighttime light observations possess distinct characteristics in their capacity to characterize urbanized regions by providing a proxy for anthropogenic activities beyond alterations in land cover (Zhao et al. 2019). Currently, there exist a variety of nighttime light -based urban extent products, and this study used the latest product created by Zhao et al. (2022) based on the harmonized nighttime light time-series composites.

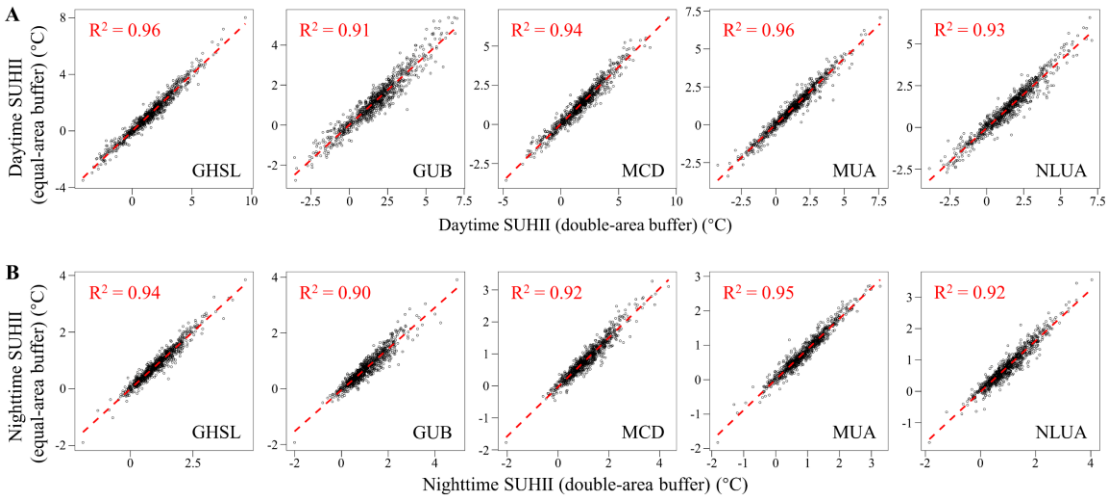

Fig. A.1. Comparison of SUHII estimated from different sizes of rural areas. (A) Annual daytime results. (B) Annual nighttime results. Double-area buffer refers to the rural area twice the size of the central urban area. Equal-area buffer refers to the rural area equal in size to the central urban area.

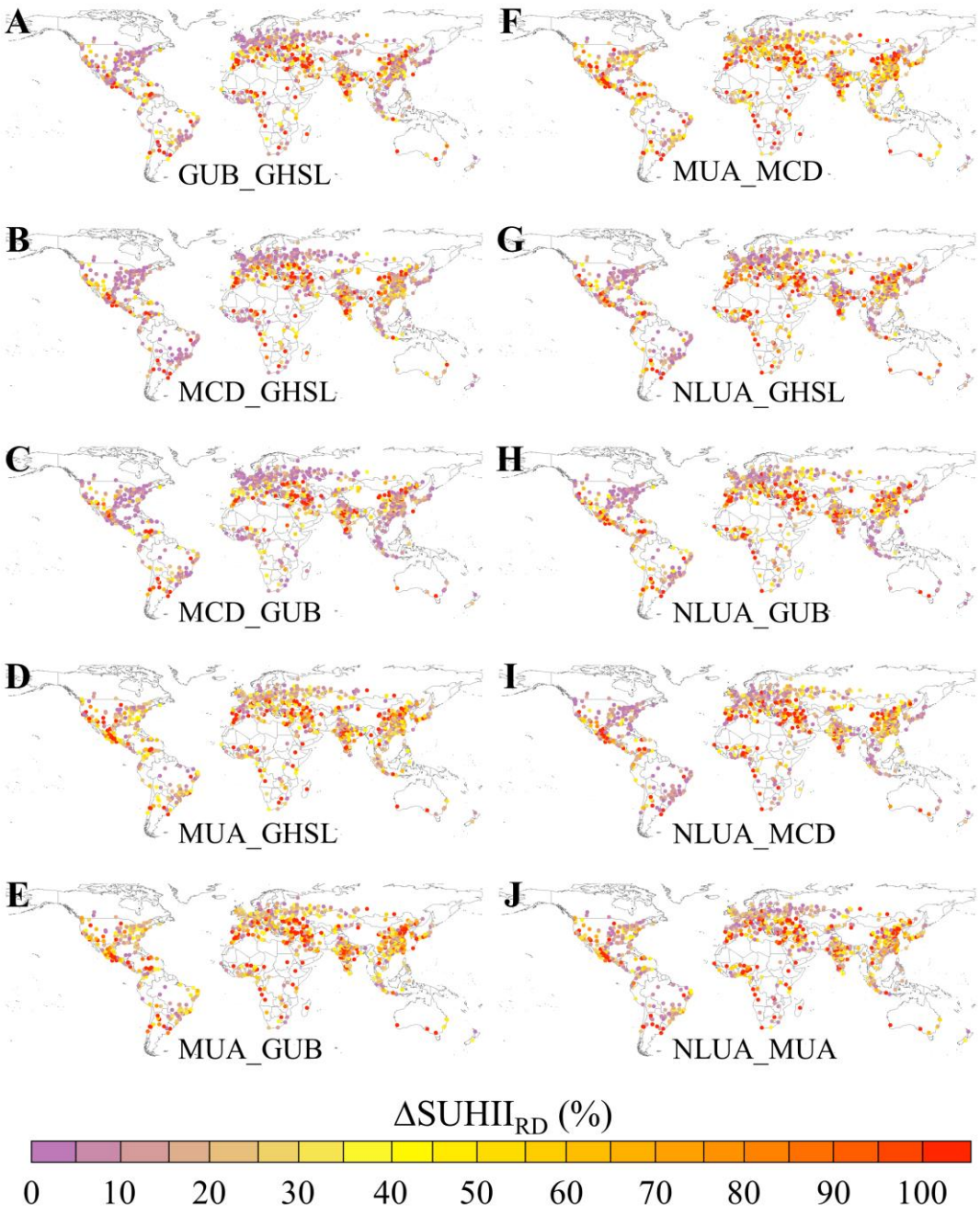

Fig. A.2. Global spatial distribution of annual daytime ΔSUHII$_{RD}$. ΔSUHII$_{RD}$ represents the relative difference in SUHII between global urban extent products.

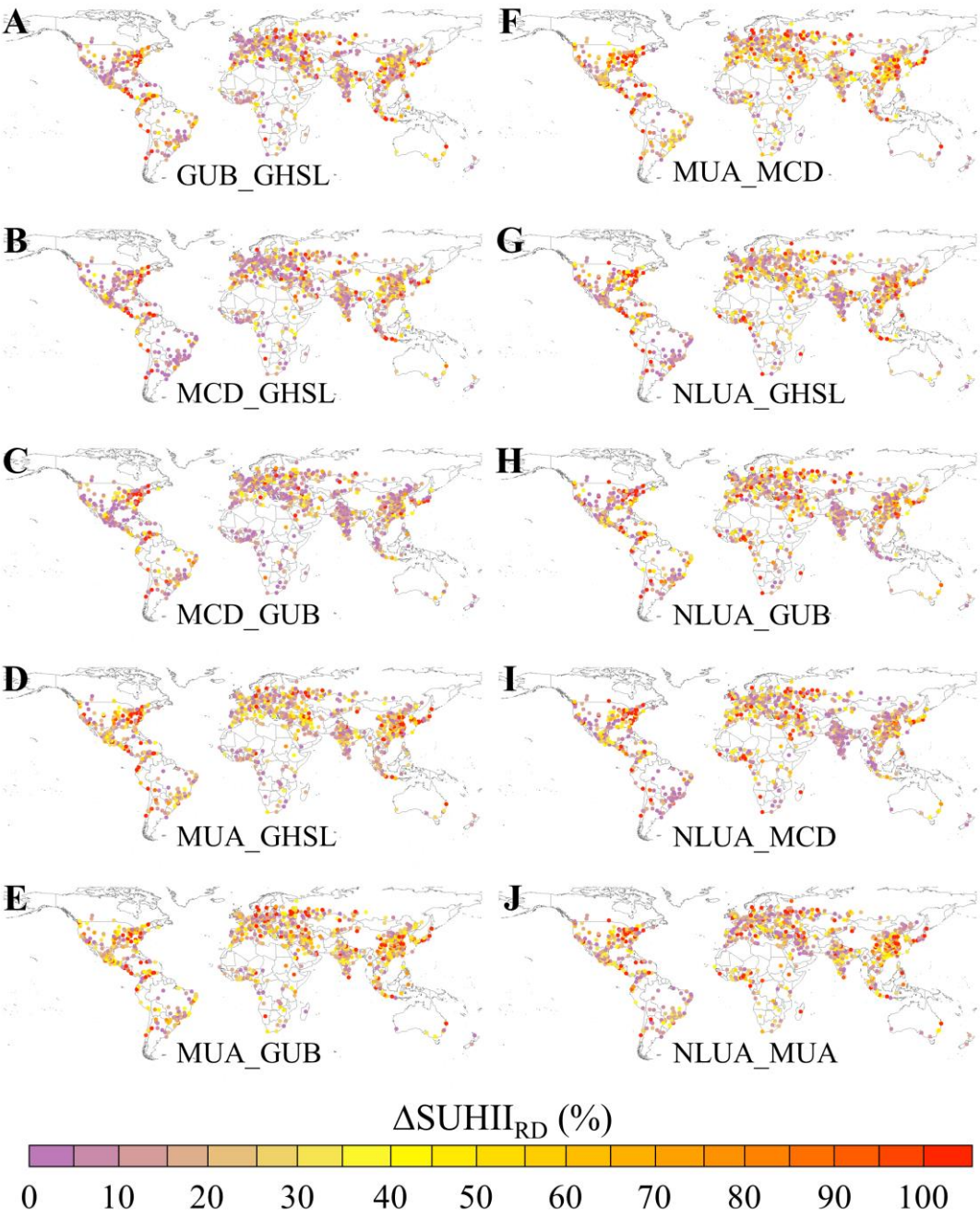

Fig. A.3. Global spatial distribution of annual nighttime $\Delta SUHII_{RD}$. $\Delta SUHII_{RD}$ represents relative difference in SUHII between global urban extent products.

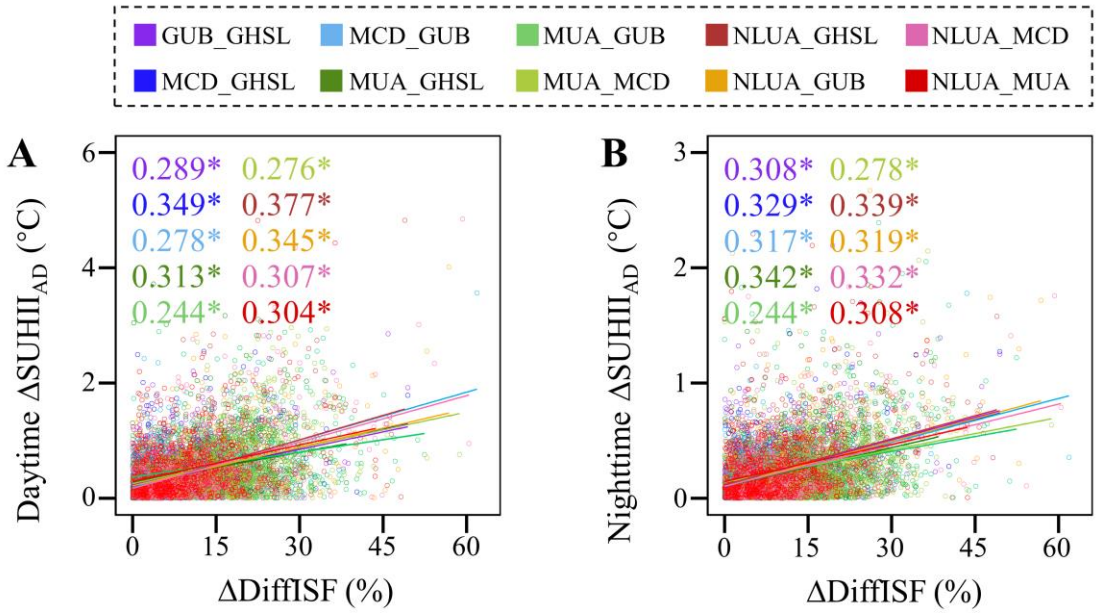

Fig. A.4. Associations between $\Delta SUHII_{AD}$ and ΔDiffISF across global cities. (A) Annual daytime results. (B) Annual nighttime results. $\Delta SUHII_{AD}$ represents the absolute difference in SUHII between global urban extent products (GUEPs). ΔDiffISF represents the difference in DiffISF (urban-rural difference in mean impervious surface fraction) between GUEPs. Colored numbers show the correlation coefficients between $\Delta SUHII_{AD}$ and ΔDiffISF, and asterisks (*) indicate statistically significant ($p < 0.01$).

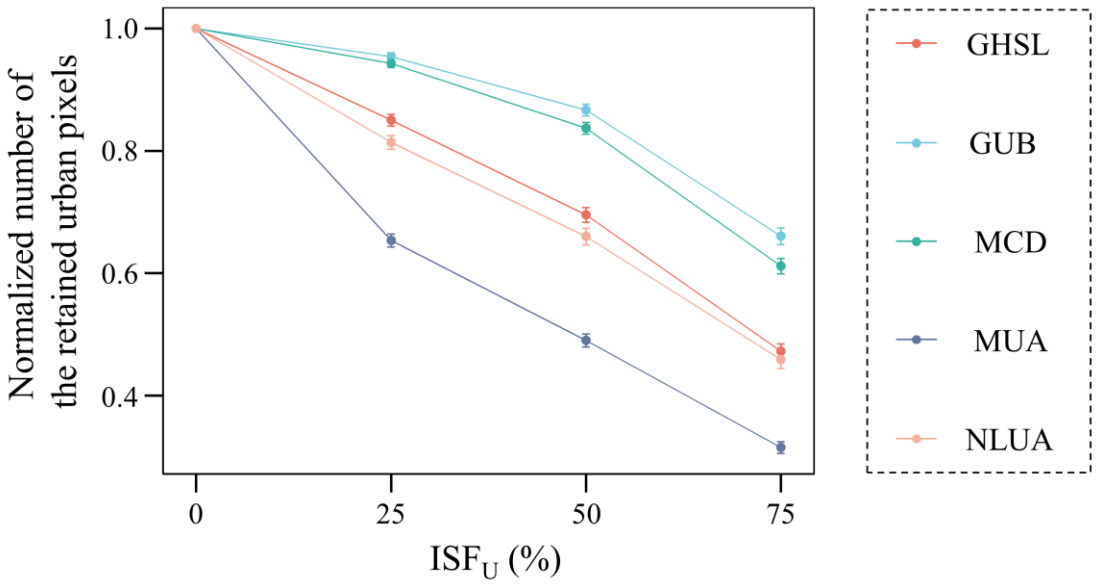

Fig. A.5. Sensitivity of the normalized number of the retained urban pixels to ISF_U of the ISF-C method. ISF_U represents the minimum impervious surface fraction (ISF) threshold of pixels that can be retained within urban extents. For comparison, number of the retained urban pixels is normalized to the initial one ($ISF_U = 0$). The colored circles and bars represent the mean values and 95% confidence intervals, respectively.

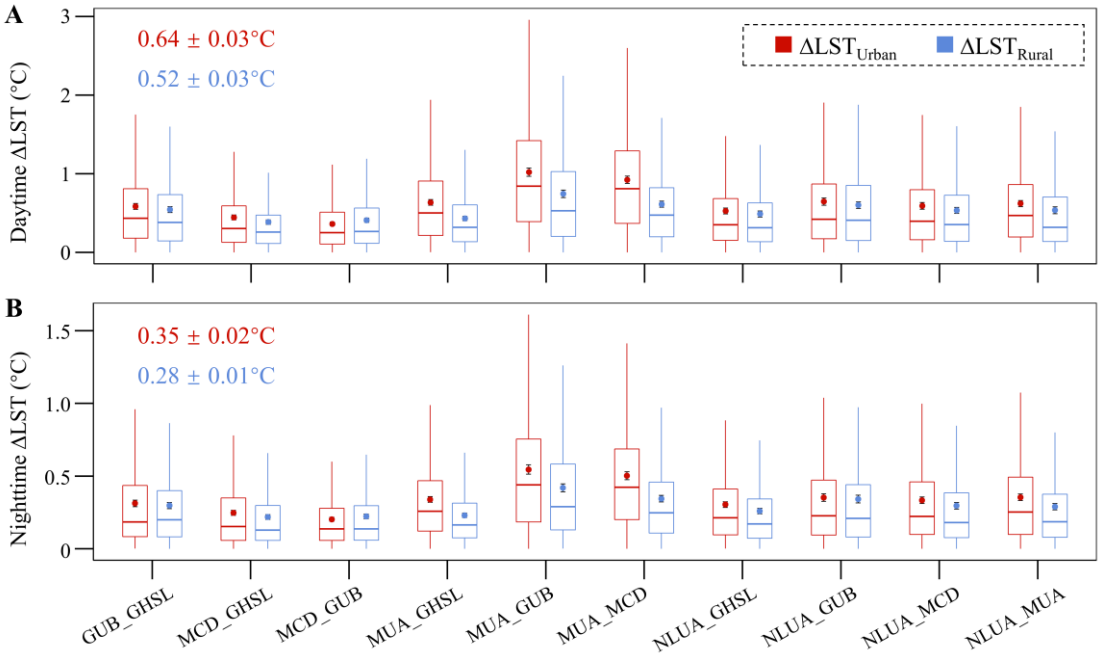

Fig. A.6. Comparison between ΔLST_{Urban} and ΔLST_{Rural}. ΔLST_{Urban} refers to the difference in urban mean LST between global urban extent products (GUEPs). (A) Annual daytime results. (B) Annual nighttime results. ΔLST_{Rural} refers to the difference in rural mean LST between GUEPs. The colored numbers (mean ± 95% confidence interval) represent the average ΔLST_{Urban} or ΔLST_{Rural} of all GUEP pairs. The central lines in the boxes are the median values. The colored circles and bars represent the mean values and 95% confidence intervals, respectively. Outliers are removed from the boxplot for presentation purposes.

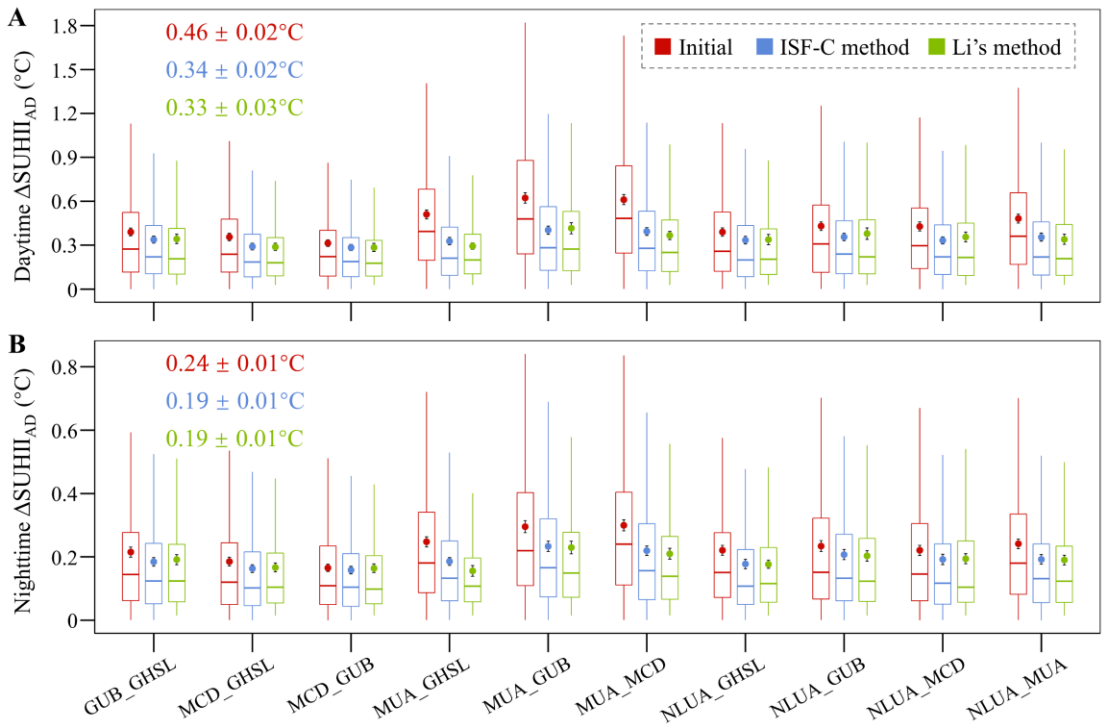

Fig. A.7. Comparison of ISF-C method and Li's method for reducing the UED-induced uncertainty in SUHII estimates. (A) Annual daytime results. (B) Annual nighttime results. $\Delta SUHII_{AD}$ represents the absolute difference in SUHII between global urban extent products (GUEPs). The colored numbers (mean ± 95% confidence interval) represent the average $\Delta SUHII_{AD}$ of all GUEP pairs. The central lines in the boxes are the median values. The colored circles and bars represent the mean values and 95% confidence intervals, respectively. Outliers are removed from the boxplot for presentation purposes.

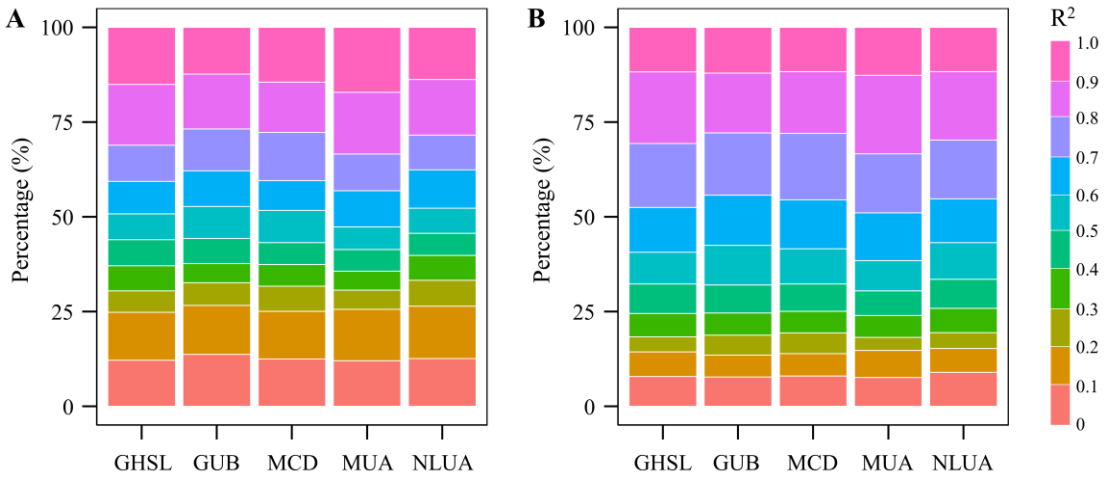

Fig. A.8. Stacked frequency distributions of R^2 for global 892 cities. (A) Annual daytime results. (B) Annual nighttime results. R^2 refers to the proportion of the variance in the land surface temperature (LST) explained by the impervious surface fraction (ISF) in a linear regression model. The range of R^2 is between 0 and 1, and a higher value indicating a better fit of the linear regression model.

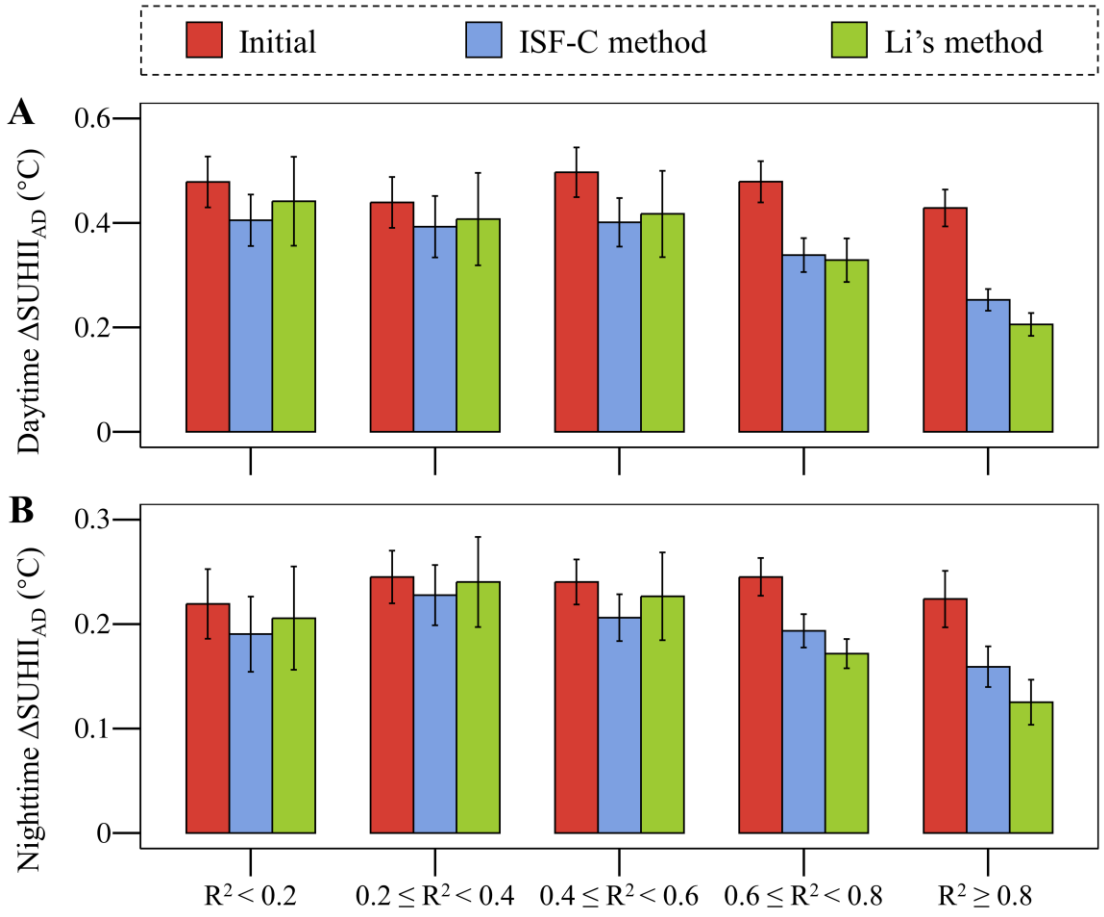

Fig. A.9. Comparison of the performance of ISF-C method and Li's method across different R^2 intervals. (A) Annual daytime average $\Delta SUHII_{AD}$ for all global urban extent products (GUEPs). (B) Annual nighttime average $\Delta SUHII_{AD}$ for all GUEPs. $\Delta SUHII_{AD}$ represents the absolute difference in SUHII between GUEPs. R^2 refers to the proportion of the variance in the land surface temperature (LST) explained by the impervious surface fraction (ISF) in a linear regression model. Error bars represent the 95% confidence intervals.

References

Chakraborty, T., Lee, X., 2019. A simplified urban-extent algorithm to characterize surface urban heat islands on a global scale and examine vegetation control on their spatiotemporal variability. Int. J. Appl. Earth. Obs. Geoinf. 74, 269-280

Clinton, N., Gong, P., 2013. MODIS detected surface urban heat islands and sinks: Global locations and controls. Remote Sens. Environ. 134, 294-304

Du, H., Zhan, W., Liu, Z., Li, J., Li, L., Lai, J., Miao, S., Huang, F., Wang, C., Wang, C., Fu, H., Jiang, L., Hong, F., Jiang, S., 2021. Simultaneous investigation of surface and canopy urban heat islands over global cities. ISPRS J. Photogramm. Remote Sens. 181, 67-83

Florczyk, A.J., Corbane, C., Schiavina, M., Pesaresi, M., Maffenini, L., Melchiorri, M., Politis, P., Sabo, F., Freire, S., Ehrlich, D., 2019. GHS Urban Centre Database 2015, multitemporal and multidimensional attributes. R2019A European Commission, Joint Research Centre (JRC)[Dataset]

Gong, P., Li, X., Wang, J., Bai, Y., Chen, B., Hu, T., Liu, X., Xu, B., Yang, J., Zhang, W., Zhou, Y., 2020. Annual maps of global artificial impervious area (GAIA) between 1985 and 2018. Remote Sens. Environ. 236, 111510

Hu, J., Yang, Y., Zhou, Y., Zhang, T., Ma, Z., Meng, X., 2022. Spatial patterns and temporal variations of footprint and intensity of surface urban heat island in 141 China cities. Sustain. Cities Soc. 77, 103585

Li, X., Gong, P., Zhou, Y., Wang, J., Bai, Y., Chen, B., Hu, T., Xiao, Y., Xu, B., Yang, J., Liu, X., Cai, W., Huang, H., Wu, T., Wang, X., Lin, P., Li, X., Chen, J., He, C., Li, X., Yu, L., Clinton, N., Zhu, Z., 2020. Mapping global urban boundaries from the global artificial impervious area (GAIA) data. Environ. Res. Lett. 15, 094044

Liao, Y., Shen, X., Zhou, J., Ma, J., Zhang, X., Tang, W., Chen, Y., Ding, L., Wang, Z., 2022. Surface urban heat island detected by all-weather satellite land surface temperature. Sci. Total Environ. 811, 151405

Liu, Z., Lai, J., Zhan, W., Bechtel, B., Voogt, J., Quan, J., Hu, L., Fu, P., Huang, F., Li, L., Guo, Z., Li, J., 2022a. Urban Heat Islands Significantly Reduced by COVID-19 Lockdown. Geophys. Res. Lett. 49

Liu, Z., Zhan, W., Lai, J., Bechtel, B., Lee, X., Hong, F., Li, L., Huang, F., Li, J., 2022b. Taxonomy

of seasonal and diurnal clear-sky climatology of surface urban heat island dynamics across global cities. ISPRS J. Photogramm. Remote Sens. 187, 14-33

Peng, S., Piao, S., Ciais, P., Friedlingstein, P., Ottle, C., Breon, F.M., Nan, H., Zhou, L., Myneni, R.B., 2012. Surface urban heat island across 419 global big cities. Environ. Sci. Technol. 46, 696-703

Sulla-Menashe, D., Friedl, M.A., 2018. User guide to collection 6 MODIS land cover (MCD12Q1 and MCD12C1) product. USGS: Reston, VA, USA 1, 18

Taubenböck, H., Weigand, M., Esch, T., Staab, J., Wurm, M., Mast, J., Dech, S., 2019. A new ranking of the world's largest cities—Do administrative units obscure morphological realities? Remote Sens. Environ. 232, 111353

Tuholske, C., Caylor, K., Funk, C., Verdin, A., Sweeney, S., Grace, K., Peterson, P., Evans, T., 2021. Global urban population exposure to extreme heat. Proc. Natl. Acad. Sci. U.S.A. 118

Venter, Z.S., Chakraborty, T., Lee, X., 2021. Crowdsourced air temperatures contrast satellite measures of the urban heat island and its mechanisms. Sci. Adv. 7, eabb9569

Yang, Q., Huang, X., Yang, J., Liu, Y., 2021. The relationship between land surface temperature and artificial impervious surface fraction in 682 global cities: spatiotemporal variations and drivers. Environ. Res. Lett. 16, 024032

Yao, R., Wang, L., Huang, X., Gong, W., Xia, X., 2019. Greening in rural areas increases the surface urban heat island intensity. Geophys. Res. Lett. 46, 2204-2212

Zhao, Zhou, Li, Cao, He, Yu, Li, Elvidge, Cheng, Zhou, 2019. Applications of Satellite Remote Sensing of Nighttime Light Observations: Advances, Challenges, and Perspectives. Remote Sens. 11, 1971

Zhao, M., Cheng, C., Zhou, Y., Li, X., Shen, S., Song, C., 2022. A global dataset of annual urban extents (1992–2020) from harmonized nighttime lights. Earth Syst. Sci. Data. 14, 517-534